Supplemental table 1: Relative fold-change from naïve control of each cytokine.

	IL-4*	IL-5*	IL-13*	IFN-γ*	IL-1β*	IL-6*	IL-12p70*	GM-CSF*	TNF-α*	IL-18*	Median Survival**
Naive	0.00	0.00	0.00	0.00	0.00	0.00	0.00	0.00	0.00	0.00	100
UgCl447	0.00	0.00	0.00	0.00	0.00	0.00	0.00	0.00	0.00	0.00	100
UgCl377	0.00	0.00	0.00	0.00	0.00	0.00	0.00	0.00	0.00	0.00	77
UgCl262	0.00	0.00	0.00	0.00	0.00	0.00	-0.51	0.00	0.00	0.00	82.5
UgCl438	0.00	0.00	0.00	0.00	0.00	0.00	0.00	0.00	0.00	-0.90	100
UgCl466	0.00	0.00	0.00	2.32	0.00	0.00	2.07	0.00	2.57	0.00	100
UgCl250	0.00	0.00	0.00	14.54	0.00	2.22	0.00	1.38	0.00	0.00	100
UgCl549	0.00	0.00	0.00	0.00	2.25	0.00	0.00	1.39	0.94	0.00	100
UgCl332	0.00	0.00	0.00	0.00	0.00	0.00	0.00	8.78	0.00	0.00	77
UgCl382	14.42	4.14	3.94	0.62	8.97	0.00	0.00	0.00	0.00	0.00	13
UgCl243	18.47	0.00	3.02	0.00	0.00	0.00	0.00	0.00	0.00	0.00	11
UgCl538	24.73	4.16	6.68	0.00	0.00	0.00	0.00	0.00	0.00	-0.77	18
UgCl450	21.44	4.77	4.22	1.25	12.77	6.76	0.00	0.00	2.70	4.37	10
UgCl534	0.00	3.02	0.00	0.00	5.15	20.44	0.00	0.00	0.00	0.00	18
UgCl547	6.12	2.85	0.00	0.00	7.56	17.87	0.00	0.00	0.00	0.00	19
UgCl292	10.59	2.90	0.00	0.00	6.40	0.00	0.00	0.00	0.00	0.00	46
UgCl300	18.25	12.49	6.14	34.66	12.25	20.46	0.00	1.74	3.33	5.94	15
UgCl326	16.08	6.79	22.11	0.00	41.57	5.56	0.00	0.00	0.00	0.00	4.5
UgCl468	41.84	8.75	9.71	0.00	12.86	56.12	0.90	3.88	3.05	0.00	8
UgCl546	129.60	55.27	50.24	0.00	15.63	26.07	0.00	2.82	2.46	1.26	35
KN99α	40.81	12.01	5.80	0.00	13.68	26.00	0.00	0.00	0.00	0.00	0
UgCl462	30.01	6.10	4.08	99.58	10.69	87.51	0.00	4.34	0.00	2.28	11
UgCl541	34.29	14.09	4.19	0.00	33.54	166.35	0.00	7.24	0.00	0.00	-5
UgCl357	49.60	5.83	7.10	17.35	13.92	34.69	104.84	119.05	24.38	1.78	0
UgCl360	0.00	0.00	0.00	267.76	28.34	42.97	1.05	3.66	10.19	3.42	15
UgCl495	0.00	0.00	0.00	538.60	26.56	45.28	0.00	3.07	0.14	4.90	25.5
UgCl422	0.00	5.90	0.00	835.13	44.26	81.18	2.12	0.00	17.43	32.44	-3
UgCl236	0.00	0.00	3.49	802.91	0.00	0.00	0.00	6.91	0.00	0.00	-5
UgCl535	0.00	0.00	0.00	943.10	28.43	54.53	1.12	5.04	9.01	0.00	-1.5
UgCl390	0.00	0.00	0.00	609.20	31.80	69.81	0.00	6.40	11.46	0.00	14
UgCl247	0.00	0.00	3.89	1923.82	27.92	71.07	0.00	9.23	0.00	9.48	-2

*Number is from three technical replicates each from five mice

**Median survival from 5 or 10 mice

Supplemental table 2: Ordinal categorical variables association table for ST93A GWAS from variables analyzed using a proportional odds logistic mixed model.

	Marker	Alt Freq	Alt Counts	Missing Rate	P value	beta	seBeta
L-DOPA 30°C	4_995956	0.18	6	0.15	0.0005	1.98	0.63
	6_989732	0.29	10	0.15	0.0026	-1.48	0.51
	12_503401	0.42	16	0.05	0.0047	1.24	0.44
SDS	13_11108	0.15	6	0	0.0017	2.34	0.79
	5_836479	0.25	10	0	0.0024	1.95	0.65
	1_975397	0.39	14	0.1	0.0033	1.90	0.65
Growth on 37°C	7_165873	0.35	14	0	0.0003	-1.75	0.50
	12_503049	0.16	6	0.05	0.0017	2.03	0.67
	12_15014	0.39	14	0.1	0.0019	1.68	0.55
Virulence category	9_6619	0.25	10	0	0.0014	2.63	0.84
	10_15302	0.33	12	0.1	0.0033	-1.99	0.70

Supplemental table 3: SNP and gene results from three GWASs

	ST93 all SNPs Human GWAS	ST93 all SNPs Mouse GWAS	ST93A Mouse GWAS
SNPs	207	161	108
Genes	115	75	45
Filtered SNPs+	145	127	93
Filtered genes+	40	38	32
SNPs from human and mouse		42	34
Genes from human and mouse		16	17

+ Gene with only one significant SNP associated with only one trait were filtered from analysis

Supplemental table 4: Function of genes identified in mouse GWAS

Gene	Predicted Phenotype
CNAG_00012	Hypothetical; orthology to: oxioreductase or NAD binder
CNAG_01241	Enzyme regulator
CNAG_01461	Sodium/bile acid co-transporter
CNAG_01491	Hypothetical; orthology to: ankyrin repeat protein
CNAG_02176	Hypothetical
CNAG_02475	Flavin-containing monooxygenase
CNAG_02487	*phs1*
CNAG_03387	Hypothetical
CNAG_04101	Oxidation of branched chain-fatty acids
CNAG_04922	Hypothetical
CNAG_05185	Hypothetical
CNAG_05329	*myo*-inositol 2-dehydrase
CNAG_05661	FACT complex subunit
CNAG_05662	*itr4*
CNAG_05664	Branched chain amino acid transaminase
CNAG_05746	Swiss dependent recombination DNA repair
CNAG_05913	Alpha glucosidase
CNAG_05937	Hypothetical
CNAG_05987	Hypothetical
CNAG_06169	Hypothetical; orthology to s-glutathione dioxygenase
CNAG_06256	Hypothetical
CNAG_06574	*app1*
CNAG_06876	Alpha ketoglutarate-dependent taurine dioxygenase
CNAG_07497	Hypothetical
CNAG_07528	DNA binding protein; putative transposon
CNAG_07586	Hypothetical
CNAG_07728	Solute carrier family 3a (Zinc transporter)
CNAG_07748	t-RNA methyltransferase
CNAG_07837	Hypothetical
CNAG_07874	Sugar transporter
CNAG_07950	Hypothetical
CNAG_08006	Hypothetical

Supplemental table 5: RNAseq Transcript Data

	KN99α*			*itr4Δ**		
PHS1	11.52	11.70	11.71	9.04	9.07	8.87
CNAG_04101	11.84	11.90	11.78	11.72	11.62	11.73
CNAG_05664	11.60	11.58	11.65	0.00	0.00	0.00
ITR4	14.69	14.68	14.67	0.00	0.00	0.00
CNAG_05329	8.36	8.55	8.34	8.00	7.90	8.17
CNAG_01241	10.94	11.19	11.01	11.33	11.25	11.47
CNAG_07950	3.63	2.25	2.45	2.48	4.07	2.45
CNAG_07528	4.63	3.84	4.36	3.37	4.23	5.22
CNAG_06256	-0.18	-0.07	1.45	2.84	2.79	2.71

*Average of three technical replicates

Supplemental table 6: Primers used in this study

Primer name	Sequence (5'-3')	Description
CX5	GTAAAACGACGGCCAG	M13F
CX6	CAGGAAACAGCTATGAC	M13R
JH8994	TGTGGATGCTGGCGGAGGATA	JH8994
CX249	GAGGCTATTCGGCTATGACTGG	NEO split F
CX2281	AGGCTGGCAAATCAAGCGTG	ITR4 F1
CX2282	CTGGCCGTCGTTTTACCGTGGTGATGGTGGTGCTCGAG	ITR4 R1
CX2283	GTCATAGCTGTTTCCTGACGGGGAGAAAGGCGTAGAGG	ITR4 F2
CX2284	CAACTTCCCAATACATCATG	ITR4 R2
CX1010	CTGAGATTGCTCCCGCTAGG	ITR4 F3
CX1011	AATGAACACCACCCAAGCCA	ITR4 R3
CX1009	TGCAGTTTACATTTCCAATCGTC	ITR4 F4
CX2285	CAGGTATTTGACTAGTCTGC	ITR4 R4
CX1419	TACCGAGCTCGGATCCGACTCTCACGTCGTTGTATAC	pJAF1-ITR4 F
CX1420	CGTTACTAGTGGATCCTCCAAGCACCCATCACTACATG	pJAF1-ITR4 R
CX1800	CAACATGTCTGGATCCATGTCCACGCTTGACTACAAG	pCXU200-ITR4 F
CX1801	TAGAACTAGTGGATCCAGCCTTCGACCGCTTTTCATT	pCXU200-ITR4 R
CX115	CATCGCTTCCGCATTCACTCACTC	ITR4 QPCR F
CX116	TTGCCGGTACCCTTGACGATAACA	ITR4 QPCR R
CX2365	CACCGATGGTTCATCCCTATAC	CNAG_05664 QPCR F
CX2366	GGACATAGCGTATCCCTTCTTC	CNAG_05664 QPCR R

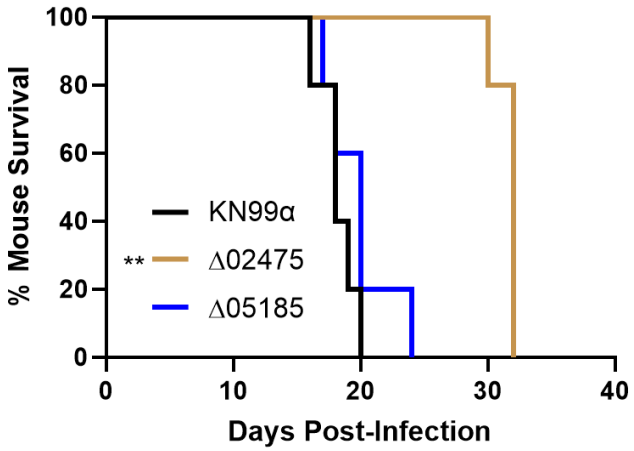

Supplemental Figure 1: Deletion mutants identified across multiple genomic studies had growth or virulence defects. Five A/J mice were infected with $5x10^4$ cells of Δ02475 and Δ05185. Significance was determined using a Gehan-Breslow-Wilcoxon test and deletion mutants were compared to KN99α (n=5; p=0.0039). Source data are provided as a Source Data file. (** = $P < 0.01$)

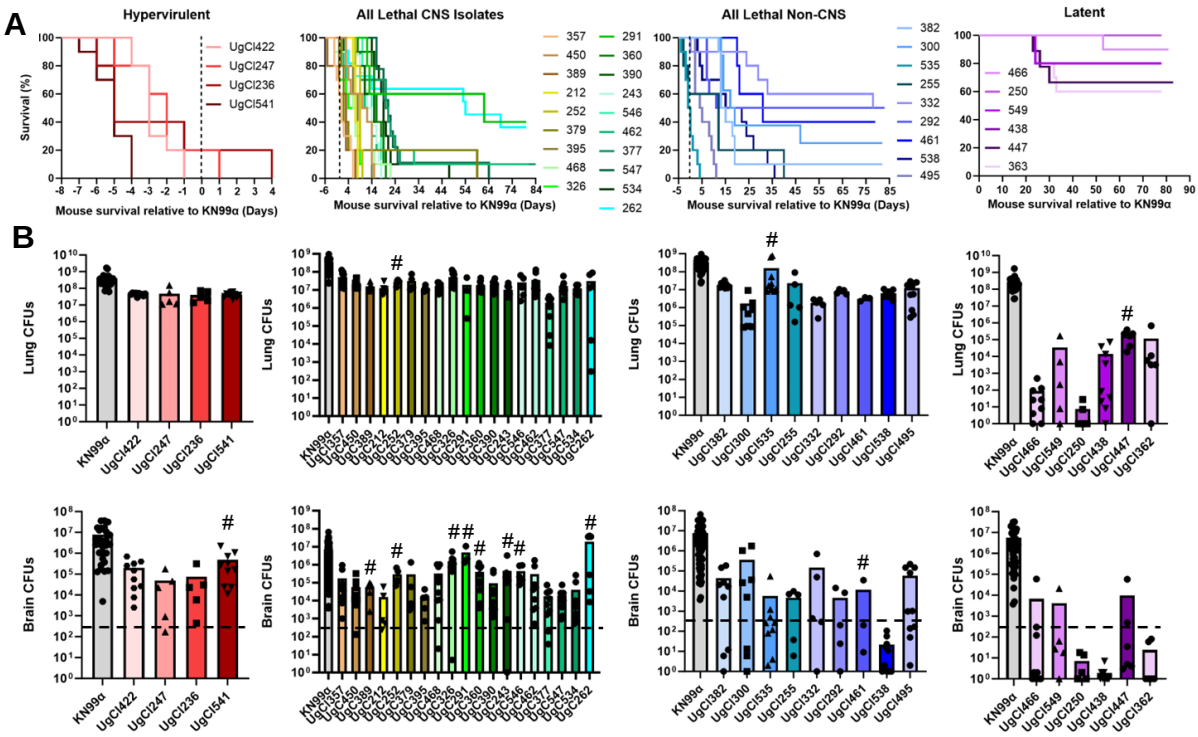

Supplemental figure 2: Mice infected with clinical isolates showed four distinct virulence manifestations. Five or 10 mice were infected with $5x10^4$ cells of each clinical isolate and monitored for 100 days. Mouse virulence was categorized into four categories, depending on relative median survival and CFUs in the mouse brain. A) All survival curves are shown. The survival curves were normalized to a matched KN99α control. B) Mouse CFUs were collected from the lungs and brain of mice at terminal endpoint. For mice infected with typical CNS, typical non-CNS, and hypervirulent isolates, CFUs are all from mice that succumbed to infection rather than mice sacrificed at 100 days post infection. For mice infected with latent isolates, the CFUs are from mice that survived to 100 days post infection. Significance was determined using Kruskal-Wallis nonparametric test with Dunn's multiple comparison correction. # marks mice that are not significantly different from the KN99α control. (n=3-10; exact P-values provided in Source Data file). Source data are provided as a Source Data file.

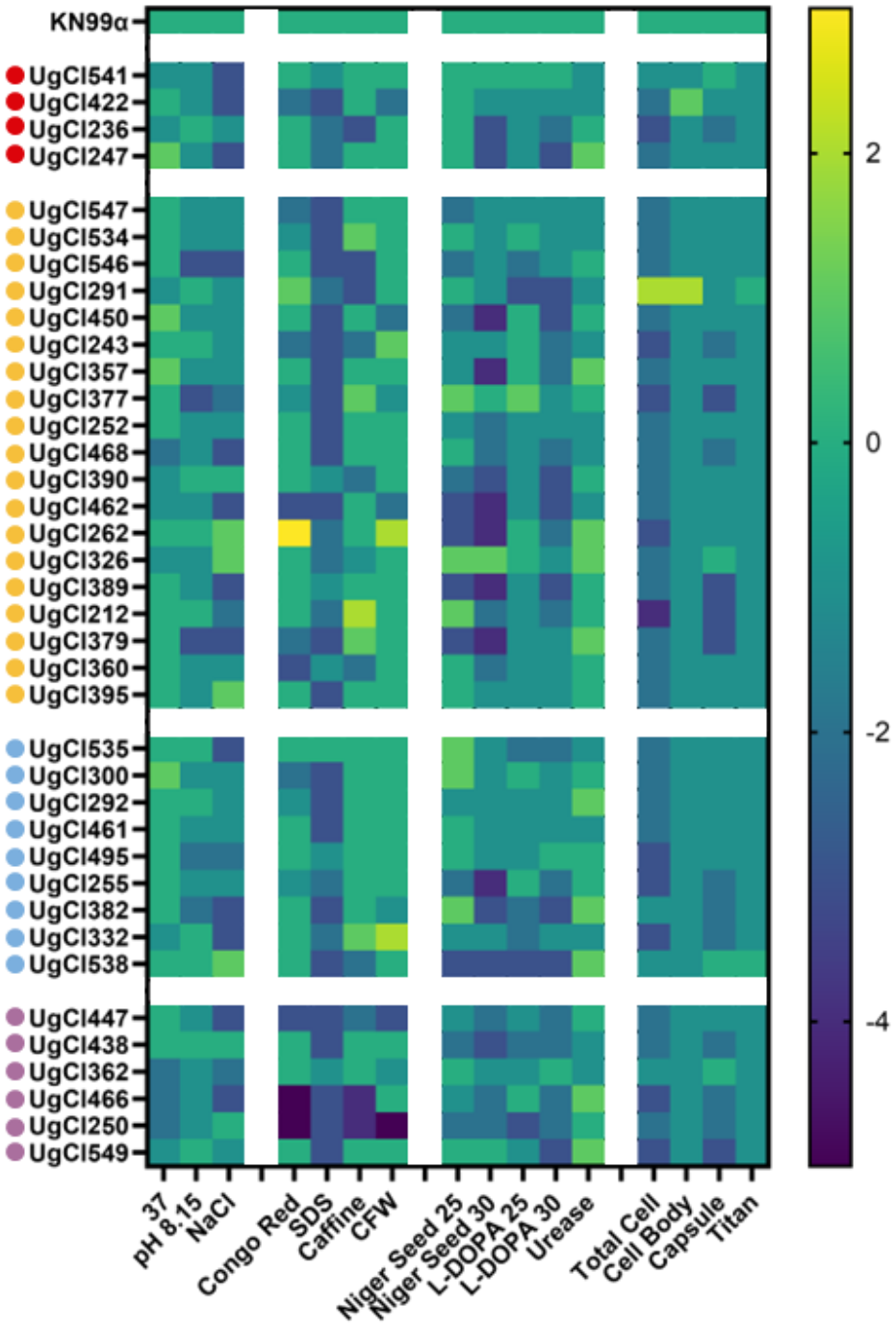

Supplemental figure 3: *in vitro* phenotypes do not correlate with disease manifestation. *in vitro* phenotype data was collected for each clinical isolate. For cell growth stressors and cell wall and membrane stressors, cells were diluted from 10^1-10^4 and spot plated in triplicate on media containing each stressor. Growth of each isolate was determined relative to growth on unadulterated YPD media. Melanin production was determined by spotting 10^6 cells in triplicate

on either Niger seed or L-DOPA plates and grown at either room temperature or at 30ºC. Each isolate was given a score of 1-5 depending on the shade of brown or black for each colony. Urease production was determined by plating 10^1-10^4 cells on Christensen's urea agar and determining the dilution at which the zone of clearance occurred. Cell morphology was determined by growing cells in water supplemented with FBS for three days (62). Cells were imaged and 200 cells from each isolate was measured to determine cell body size, capsule size, total cell size, and ability to form titan cells. Isolates were assigned a numerical score depending on each size. Sample clustering was performed using an average clustering linkage method and Euclidean distance measurement (63), and no associations were observed. Four representative isolates from each virulence category were selected and grouped manually in order of virulence. The heat map was normalized to KN99α and each isolate was compared to KN99α. Scale bar describes relative ability to grow under stress, produce effector proteins, etc. in comparison to KN99α; i.e. "more" or "less" than KN99α. In general, there were no associations between *in vitro* phenotypes and disease manifestation. Source data are provided as a Source Data file.

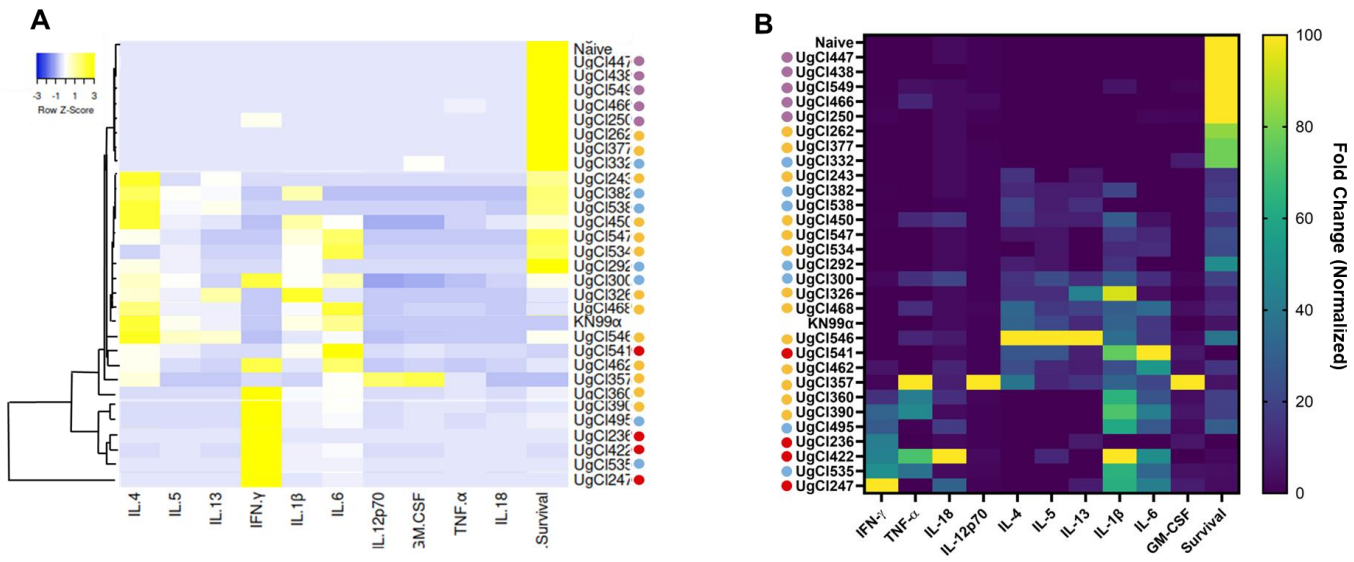

Supplemental figure 4: *in vivo* immune response associates with disease outcome. A) Sample clustering was performed using an average clustering linkage method and Euclidean distance measurement (63) and normalized by row. B) Heatmap describing the normalized fold change**.** Mice were sacrificed on day 17 or 21 post infection, and lungs removed. The lung supernatant was collected, and cytokine levels determined using ThermoFisher Th1/Th2 cytokine panel and a Luminex Magpix. The fold change from a naïve control was calculated for each sample that had a significant (P<0.05) increase in cytokines from uninfected mice. Significance was determined using Kruskal-Wallis nonparametric test with Dunn's multiple comparison correction. Sample clustering was performed using an average clustering linkage method and Euclidean distance measurement (63). The heat map was normalized. Representative samples are shown. Median survival was normalized to KN99α survival. Latent isolates (purple) clustered with the uninfected control and showed a mostly undetectable immune response. Typical CNS (yellow) and typical non-CNS (blue) isolates generally showed a type 2 immune response, with increases in IL-4, IL-5, and IL-13, and clustered with KN99α. Hypervirulent isolates (red) generally showed an increase in type 1 cytokines, including IFNγ, or

proinflammatory cytokines, including IL-1β, IL-6, and GM-CSF. Source data are provided as a Source Data file.

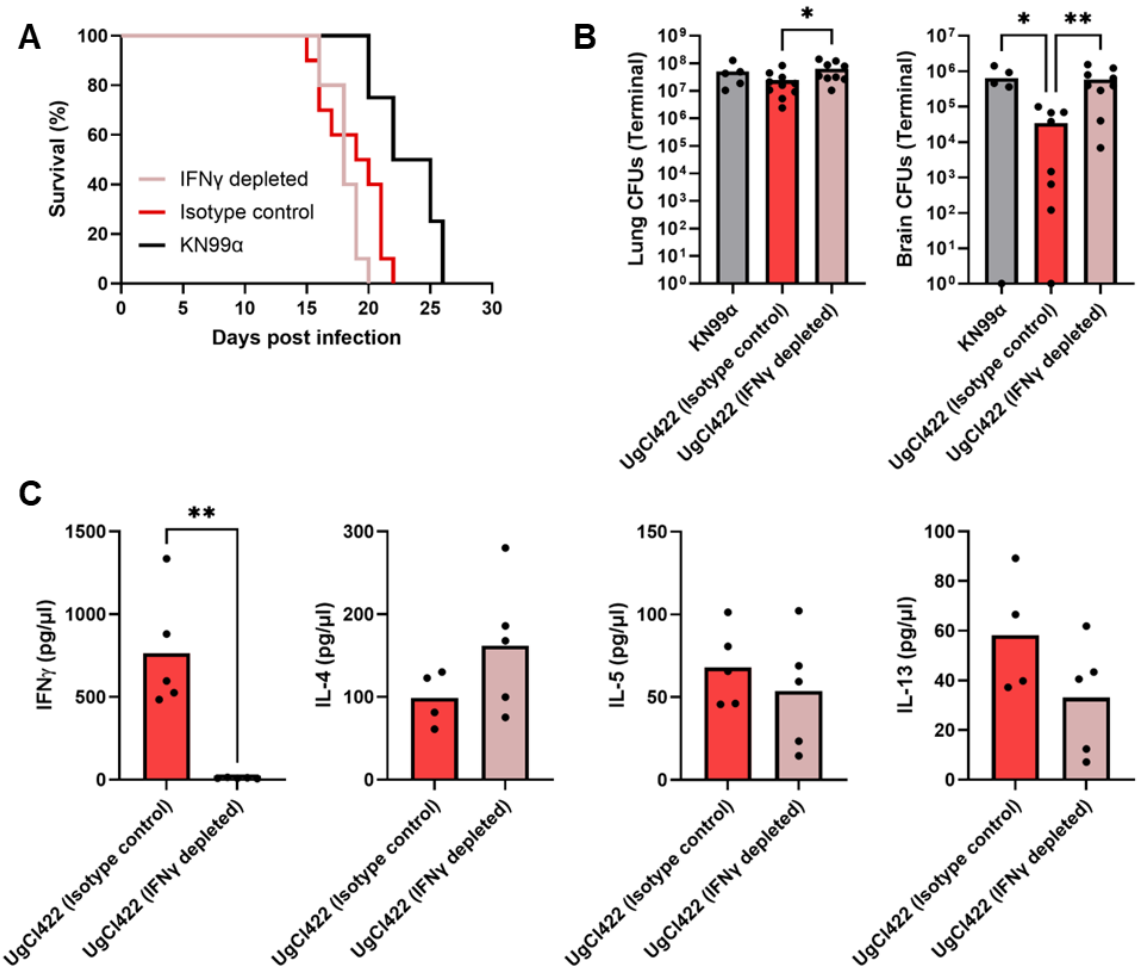

Supplemental figure 5: IFNγ depletion causes increased dissemination but does not alter survival. 10 mice were treated with IFNγ antibody and an isotype control. A) There was no impact on survival. Significance was determined with a Gehan-Breslow-Wilcoxon test and IFNγ was compared to the isotype control (P = 0.3974). B) The IFNγ depleted mice had a significant increase in lung and brain fungal burden. Significance was determined with a Kruskal-Wallis nonparametric test with Dunn's multiple comparison correction (n=10; Lung from left to right, P = 0.0281; Brain, from left to right, P = 0.0076; P = 0.0318). C) IFNγ levels were depleted in the IFNγ depletion mice, but there was no impact on type 2 immune responses. Significance was determined with a Kruskal-Wallis nonparametric test with Dunn's multiple comparison correction (n=5; P = 0.0079) Source data are provided as a Source Data file. (* = $P < 0.05$; ** = $P < 0.01$).

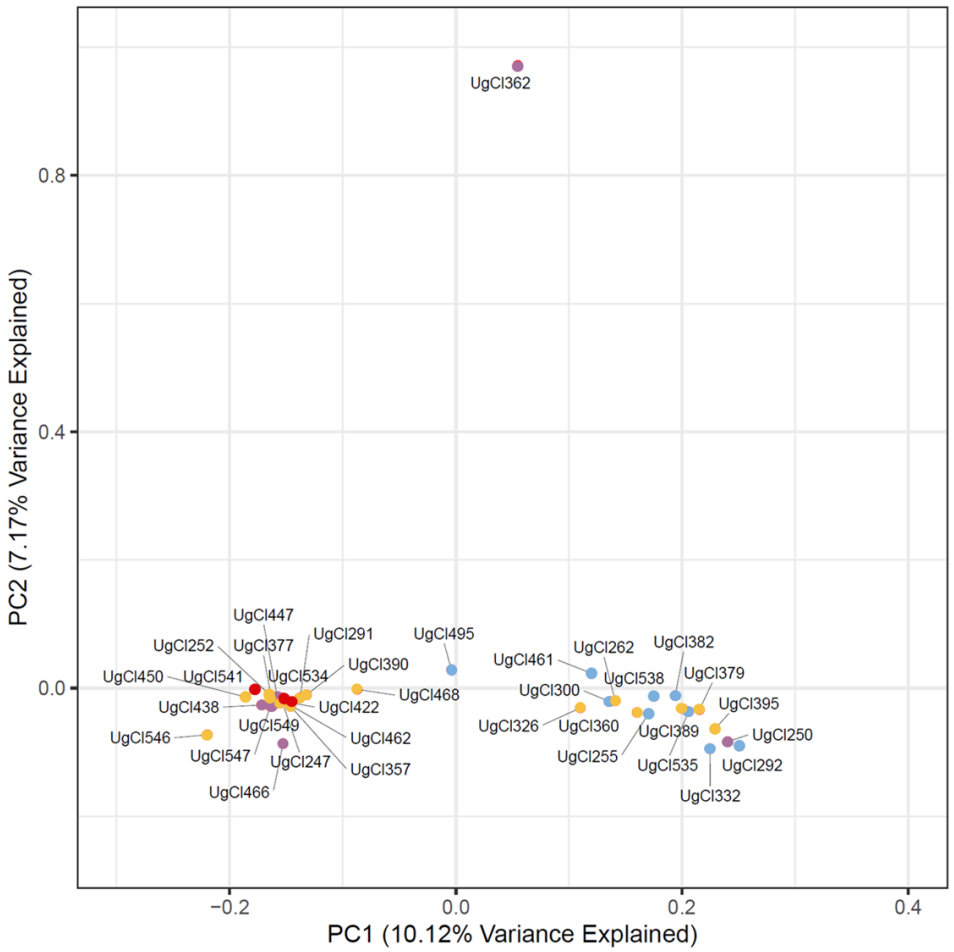

Supplemental figure 6: Principal component analysis on all mutations in the ST93 population. A PCA was performed using all SNPs/INDELs in the ST93 isolates. No clusters were observed.

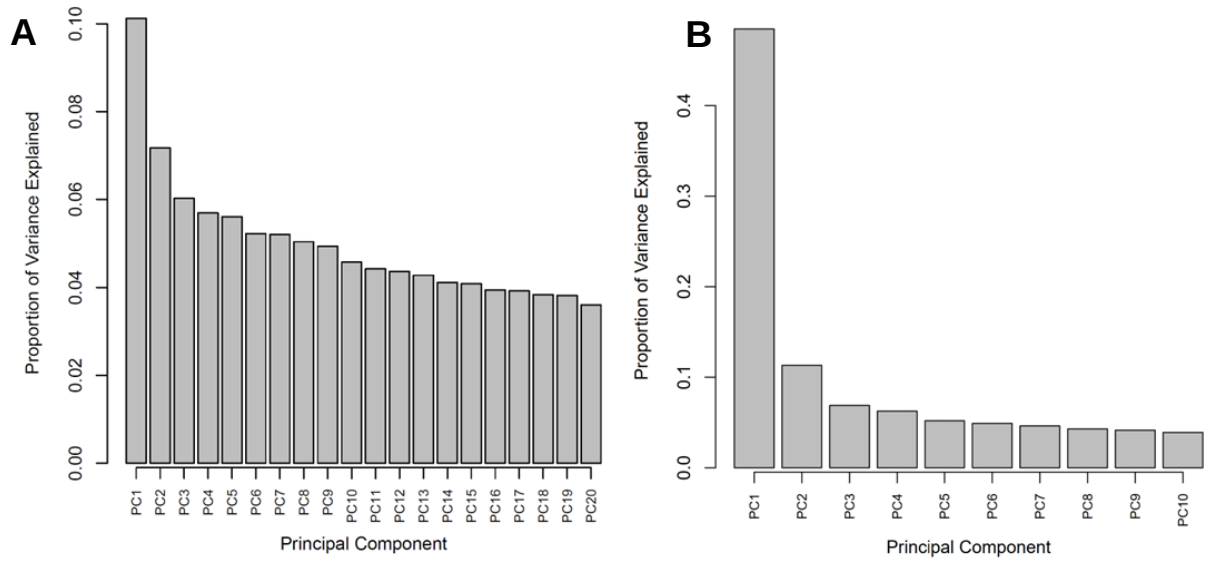

Supplemental figure 7: Variance for Principal Component Analysis. A) Scree plot for all SNPs in population. B) Scree plot for 562 SNPs predicted to influence gene coding or regulation.

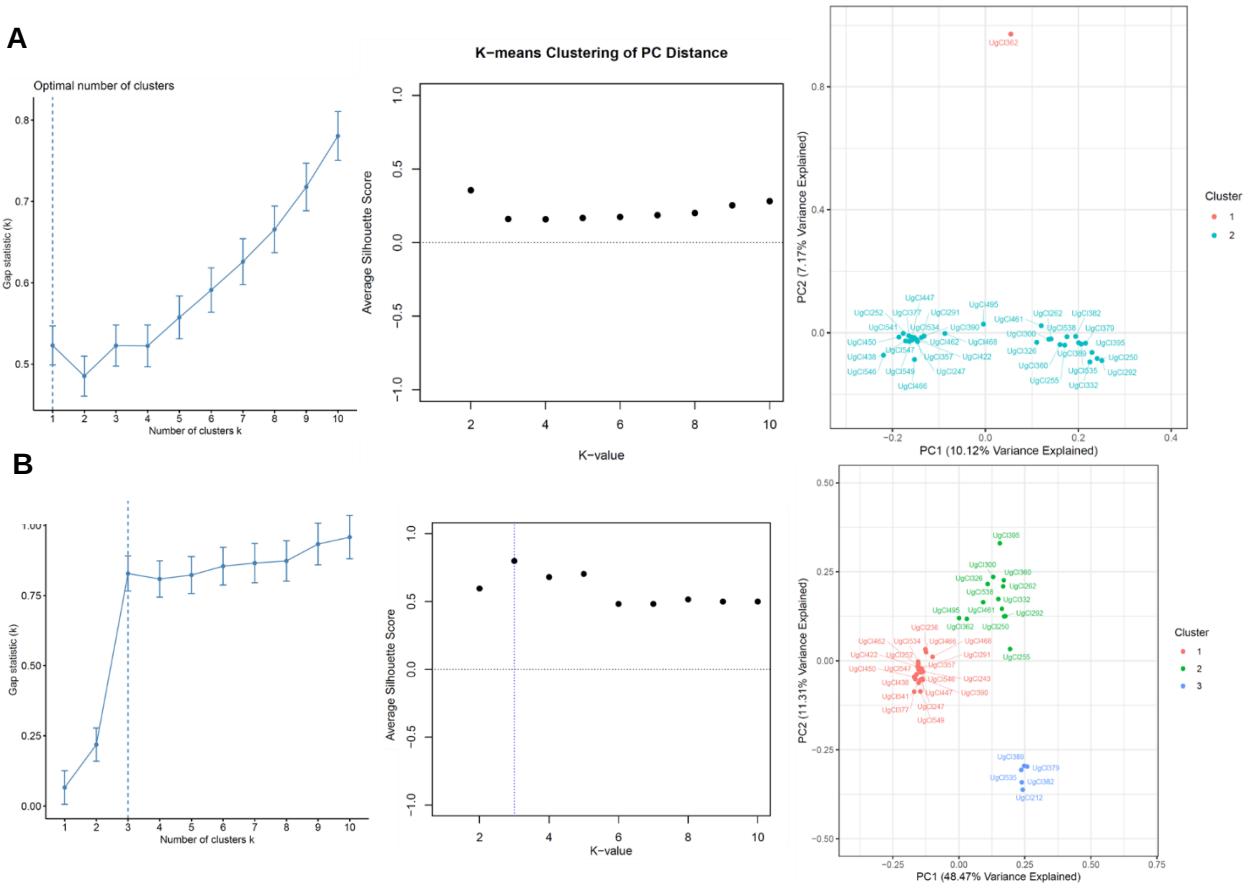

Supplemental figure 8: K-means clustering revealed three clusters of isolates. Distance between points was calculated with Euclidean distance. Gap statistic (65) and silhouette score (66) were used to calculate the ideal number of clusters. A) For all variates, gap statistic showed no clusters and K-means suggested that K=2 was the optimal number of clusters. Each isolate was colored according to the K=2 assignment. B) The coding variants found that K=3 was the optimal number of clusters. Each isolate was colored corresponding to the K=3 assignment.

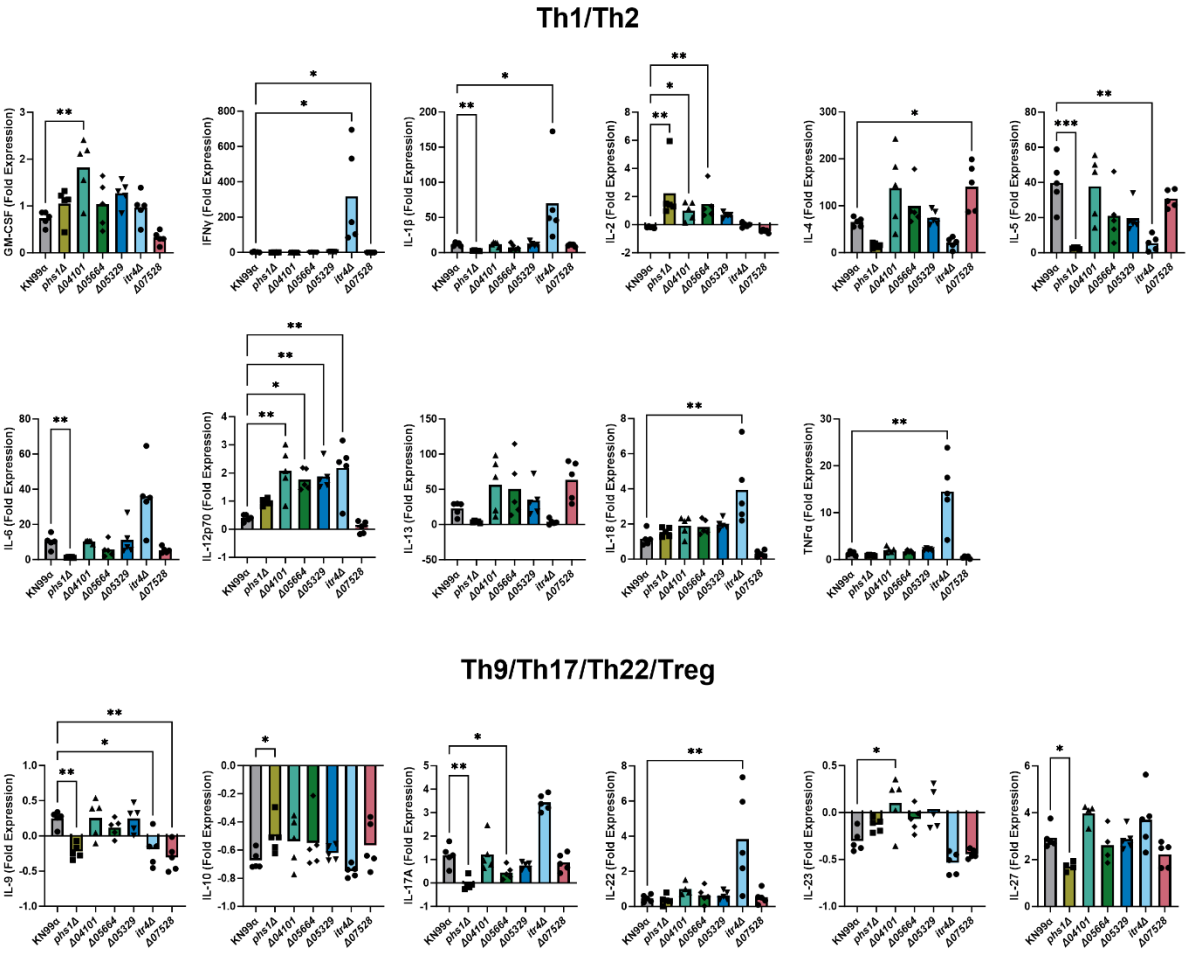

Supplemental figure 9: Cytokine results from all deletion mutants. 5 mice were sacrificed on day 17-20 post infection and lungs removed. The lung supernatant was collected, and cytokine levels determined. Fold expression was calculated relative to an uninfected control. Significance was determined using a Kruskal-Wallis nonparametric test without Dunn's multiple comparison correction (* = $P < 0.05$; ** = $P < 0.01$; *** = $P < 0.001$; n=5; exact p-values in Source Data file). Source data are provided as a Source Data file.

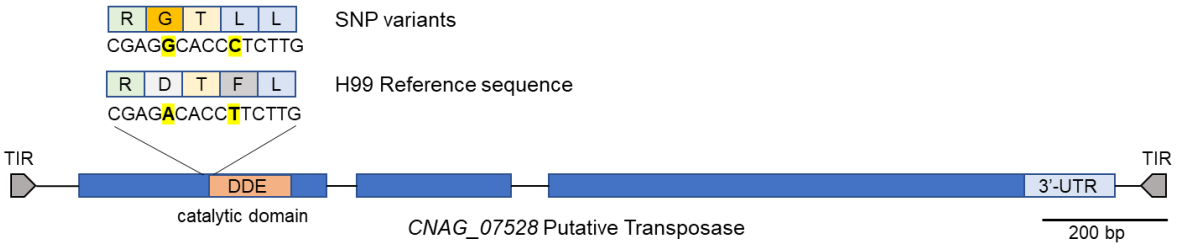

Supplemental figure 10: SNP variants (highlighted) *in CNAG_07528*, a putative DNA transposase, associated with hypervirulence in clinical isolates. Signature features of DNA transposon Class II mobile element sequences are indicated including an endonucleolytic DDE catalytic domain and putative 44-bp terminal inverted repeats (TIRs) flanking the transposase gene.